

PNNL-37408

Seismic DAS observations of a large underground chemical explosion in dry tuff

March 2025

Kirsten N. Chojnicki James T. St. Clair D. Parker Sprinkle Joshua D. Feldman PE1 Experiment Team



DISCLAIMER

This report was prepared as an account of work sponsored by an agency of the United States Government. Neither the United States Government nor any agency thereof, nor Battelle Memorial Institute, nor any of their employees, makes any warranty, express or implied, or assumes any legal liability or responsibility for the accuracy, completeness, or usefulness of any information, apparatus, product, or process disclosed, or represents that its use would not infringe privately owned rights. Reference herein to any specific commercial product, process, or service by trade name, trademark, manufacturer, or otherwise does not necessarily constitute or imply its endorsement, recommendation, or favoring by the United States Government or any agency thereof, or Battelle Memorial Institute. The views and opinions of authors expressed herein do not necessarily state or reflect those of the United States Government or any agency thereof.

PACIFIC NORTHWEST NATIONAL LABORATORY

operated by

BATTELLE

for the

UNITED STATES DEPARTMENT OF ENERGY

under Contract DE-AC05-76RL01830

Printed in the United States of America

Available to DOE and DOE contractors from the Office of Scientific and Technical Information, P.O. Box 62, Oak Ridge, TN 37831-0062

www.osti.gov ph: (865) 576-8401 fox: (865) 576-5728 email: reports@osti.gov

Available to the public from the National Technical Information Service 5301 Shawnee Rd., Alexandria, VA 22312 ph: (800) 553-NTIS (6847) or (703) 605-6000

email: info@ntis.gov
Online ordering: http://www.ntis.gov

Seismic DAS Observations of a large underground chemical explosion in dry tuff

March 2025

Kirsten N. Chojnicki James T. St. Clair D. Parker Sprinkle Joshua D. Feldman PE1 Experiment Team

Prepared for the U.S. Department of Energy under Contract DE-AC05-76RL01830

Pacific Northwest National Laboratory Richland, Washington 99354

Abstract

On 18 October 2023 a 16.3-ton TNT equivalent chemical explosion was detonated underground at the Nevada National Security Site, generating a seismic event (Meyers et al., 2024). The associated seismic wavefield was measured on a Distributed Acoustic Sensing (DAS) array with slant range distances from 27 m - 1123 m. The first arriving phase traveled at an apparent velocity of about 2640 m s⁻¹ from 27 m to 420 m slant range and about 2470 m s⁻¹ from 505 m to 1123 m slant range according to the first arrival moveouts on the DAS data. The first arrival from the explosion temporarily saturated the cable from a slant range of 27 m - 186 m and 0.009 s to 0.084 s post detonation. From 186 m slant range to 420 m slant range, peak strain rates of 5.6 x 10⁶ nm m⁻¹ s⁻¹ were observed for the first arrival phase. For the first arrival from 505 m slant range to 1123 m slant range, peak strain rates reduced to 8.0 x 10⁴ nm m⁻¹ s⁻¹. A comparison of the scaled accelerations computed from DAS, the geophone pairs, and the measurements of co-located accelerometer pairs show common agreement at the scaled ranges of the single point sensors. This study adds to the body of work reporting near-source DAS observations of the seismic wavefields generated by underground chemical explosions. These results indicate that near-source DAS observations can refine interpretations of phase identification from singlepoint sensor observations. Phase identification could be one mechanism that contributes scatter to single point seismic measurements which would confound the performance of empirical relationships for small explosions. Removing that mechanism may therefore reduce interstation variability and increase empirical relationship performance for small explosions.

Abstract

Acknowledgments

This Low Yield Nuclear Monitoring (LYNM) research was funded by the National Nuclear Security Administration, Defense Nuclear Nonproliferation Research and Development (NNSA DNN R&D). The authors acknowledge important interdisciplinary collaboration with scientists and engineers from LANL, LLNL, NNSS, PNNL, and SNL. This work was heavily supported by MSTS for the installation of the DAS cables. The authors express extreme gratitude to Silixa, LTD for support with design, installation and acquisition of DAS data discussed in this report. The authors wish to thank Reagan Turley and Bob White of MSTS for support installing and maintaining the geophones and accelerometers. The authors wish to thank UNR for support with the geophone and accelerometer telemetry and data retrieval.

Acknowledgments

* PE1 Team

Myers, S.C.¹, Abbott, G.⁶, Alexander, T.², Alger, E.¹, Alvarez, A.⁵, Antoun, T.¹, Graham, A.⁶, Banuelos, H.5, Barela, M.3, Barnhart, T.3, Barrow, P.4, Bartlett, T.5, Bockman, A.1, Bodmer, M.4, Bogolub, K.⁷, Bonner, J.¹¹, Borden, R.⁴, Boukhalfa, H.³, Bowman, D.⁴, Britt, C.², Broman, B.⁹, Broome, S.⁴, Brown, B.⁵, Burghardt, J.², Chester, D.⁶, Choens, C.⁴, Chojnicki, K.², Churby, A.¹, Cole, J.³, Coleman, T.⁹, Collard, J.⁶, Couture, A.², Crosby, G.¹, Cruz-Cabrera, A.⁴, D'Saint Angelo, D.⁵, Walter, D.¹, DeVisser, B.⁵, Dietel, M.⁵, Downs, C.⁴, Downs, N.⁵, Dzenitis, E.¹, Eckert, E.⁵, Eras, S.⁴, Euler, G.³, Ezzedine, S.¹, Fast, J.², Feldman, J.², Featherston, K.⁵, Foxe, M.², Freimuth, C.⁵, Fritz, B.2, Galvin, G.6, Gamboa, S.5, Garner, L.5, Gascoigne, T.5, Gastelum, J.2, Gaylord, J.1, Gessey, D.5, Glasgow, B.², Glomski, A.¹, Goodwin, M.⁶, Green, D.⁶, Griego, J.⁴, Grover, S.⁵, Gutierrez, J.³, Haas, D.8, Hall, R.3, Hall, A.1, Hardy, D.5, Hauk, D.2, Heath, J.4, Holdcroft, J.6, Holland, A.4, Honjas, W.7, Howard, K.³, Hudson, C.⁸, Ingraham, M.⁴, Jaramillo, J.⁴, Jenkins, A.⁶, Johnson, C.², Jones, K.⁴, Falliner, J.⁴, Junor, W.³, Keillor, M.², Kent, G.⁷, Keogh, M.⁵, Kibikas, W.⁴, Leadbeater, K.⁶, Knox, H.², Knox, J.², Kuhlman, K.⁴, Kwiatkowski, C.³, Laintz, K.³, Lapka, J.⁸, Larotonda, J.⁵, Layne, J.³, Ledoux, N.³, Li, S.³, Linneman, D.², Lipkowitz, P.⁵, Malach, A.⁴, MacLeod, G.³, McCann, E.², McCombe, R.³, Meierbachtol, C.³, Mellors, R.¹, Memmot, B.⁵, Mendenhall, W.⁹, Mendez, J.², Miller, X.⁵, Miller, A.⁵, Miranda, F.⁵, Montano, M.⁴, Moore, M.², Morris, J.¹, Munley, W.², Murillo, E.5, Musa, D.3, Myers, T.4, Navarro, A.2, Nippress, S.6, Otto, S.3, Peacock, S.6, Pemberton, S.3, Perea, R.², Peterson, J.², Le Bas, P.³, Plank, G.⁷, Podrasky, A.⁹, Podrasky, D.⁹, Pope, J.⁴, Poskey, M.⁵, Powell, M.⁴, Price, A.¹, Puyleart, A.², Quintana, B.³, Rahn, T.³, Rendon, C.⁵, Reppart, J.⁵, Rico, H.5, Roberts, B.4, Robey, E.4, Rodd, R.1, Rodriguez, M.4, Rogall, A.3, Romanczuk, A.1, Roth, M.2, Salver, G.5, Savran, B.7, Schalk, W.10, Seifert, C.2, Seitz, D.3, Shao, X.3, Sirota, D.2, Slack, J.2, Slater, D.7, Smith, K.7, Smith, D.5, Spears, B.3, Sprinkle, D.2, Stead, R.3, Stephens, M.5, St Clair, J.2, Strickland, C.², Tafoya, A.³, Tafoya, J.⁴, Tagoe, M.⁵, Taguba, C.², Tarnecki, L.³, Tatge, R.⁵, Teich-McGoldrick, S.⁴, Terry, B.⁶, Thompson, R.⁵, Townsend, M.⁵, Tubbs, G.³, Turley, R.⁵, Valdez, N.⁴, Van Morris, A.², Vergara, S.⁵, Vigil, J.³, Villanueva, J.⁵, Vorobiev, O.¹, Wallace, D.³, Walrath, T.³, Wharton, S.¹, White, R.⁵, White, H.⁶, Whitehill, A.², Williams, M.⁴, Wilson, J.⁴, Wood, L.², Wright, C.3, Wright, A.4, Xu, G.4, Yang, X.1, Yost, R.3, Zeiler, C.5, Zionce, E.2

Abstract

¹ Lawrence Livermore National Laboratory

² Pacific Northwest National Laboratory

³ Los Alamos National Laboratory

⁴ Sandia National Laboratories

⁵ Nevada National Security Site

⁶ Atomic Weapons Establishment

⁷ University of Nevada Reno

⁸ University of Texas at Austin

⁹ Silixa

¹⁰ National Oceanic and Atmospheric Administration

¹¹ Desert Research Institute

Acronyms and Abbreviations

DAS Distributed Acoustic Sensing

Hz Hertz

km kilometer kT kiloton

LYNM Low-Yield Nuclear Monitoring

m meter

NEM Nuclear Explosion Monitoring NNSS Nevada National Security Site

NPE Non-Proliferation Experiment

PE1 Physics Experiment 1

PE1-A Experiment A in the Physics Experiment 1 series

RAID Redundant Array of Independent Disks

TNT Trinitrotoluene

Contents

Abstr	act		ii	
Ackn	owledg	ments	iii	
Acror	nyms a	nd Abbreviations	iv	
1.0	Unde	erground Chemical Explosions	Error! Bookmark not defined.	
2.0	DAS	2		
3.0	DAS for the PE1 Series		3	
	3.1	Design	3	
	3.2	Installation	5	
4.0	DAS Data for PE1-A		13	
	4.1	Acquisition	13	
	4.2	Processing	13	
	4.3	Signal Confirmation	14	
	4.4	System Performance	16	
	4.5	Time Series	17	
	4.6	Spectral Amplitude	20	
5.0	DAS Exploration of PE1-A Explosion Phenomenolog		ıy22	
6.0	Late	Late time observations2		
7.0	Summary and Conclusion2			
8.0	References			

Figures

Figure 1.	A map showing the DAS fiber installation that was used to record the PE1-A explosion in P-tunnel complex of the NNSS. Straight and helical DAS cables were installed in the P-Main and .06 Bypass drifts and shallowly buried in the tunnel floor from a scaled range of 27 m to 1123 m for PE1-A. The colormap represents the slant range to the center of the explosion for PE1-A, denoted with a yellow star. Locations where the cable was spliced are shown in triangles and co-located geophone and accelerometer pairs are shown in circles. A topographic map of Aqueduct Mesa underlays the tunnel map to indicate Aqueduct Mesa above the tunnel complex.	4
Figure 2.	Cross-sectional schematic of cable placement in existing trench in P-Main	5
Figure 3. Photo	tographs of the emplacement process for cable in P-Main draft showing the (a) yellow cable jackets of the fiber on the reels on rail car;, (b) staff pulling the cable off the reels; (c) laying the cable on the ground next to the trench; (d) laying the cable in the trench; (e) cables spaced within trench; and (f) trench filled with sand. Photos by K. Chojnicki.	6
Figure 4. Phot	tographs of the emplacement of the cable in sections with rails in the P-Main drift showing (a) the pre-existing trench in the P-Main drift that was leveraged for this installation; (b) the cables laid across the rails prior to being routed under the rails; (c) the areas the rails cross the trench; and (d) the cables once they were installed in the trench. Photos by K. Chojnicki	7
Figure 5. Phot	tographs showing the areas where cables in P-Main were routed; (a) out of a trench over an existing piece of infrastructure, and then down back into the trench; (b) the panduit (white material) that was installed to guide the cable; and (c) sandbags placed on top of the conduit. Photos by K. Chojnicki.	8
Figure 6. Phot	tographs of the emplacement in the .06 Bypass drifts showing (a) cable reels on rail cars, (b) staff pulling the cable off the reel, (c) guiding the cable into the trench, and (d) the final placement of the cable in the trench. Photos by K. Chojnicki.	9
Figure 7. Phot	tographs showing an example of cables being routed around existing infrastructure in the tunnel by (a) digging a trench below this pre-existing cable conduit, and then (b, c, d) routing the cable under the conduit(s). Photos by K. Chojnicki.	10
Figure 8. Phot	tographs showing the installation process of the cable down bore holes, including (a) the cable and the apex loop cable guide secured to the cable guide; (b) the cable guide being inserted downhole; (c) the cable completely installed downhole; and (d) the completion of grout in the borehole. Photos by PE1 Experiment Team	11
Figure 9. Phot	tographs showing the (a) co-located geophone and accelerometer installations; (b) an example geophone and accelerometer; and (c) an example digitizer and the power source. Photos by K. Choinicki	12

Figures vi

Figure 10.	The (a) trace normalized strain rate and (b) frequency content as a function of slant range for the straight DAS cable in the first 1.5 seconds after the explosion. The data are low pass filtered at 200 Hz. The data were saturated from 27 m – 186 m slant range as indicated by the incoherent phase and broad-band frequency response in that region. Areas with known infrastructure contribute noise around 256 m, 585 m, 645 m, 667 m, 685 m, 717 m, and 755 m slant range (see text for more information).	15
Figure 11.	Strain rate as a function of time measured from DAS (blue line) and computed from the geophone (orange line) and accelerometer (gold line) pairs at 596 m, 857 m, and 997 m slant range.	17
Figure 12.	Peak strain rates induced on the cable from the detonation of PE1-A reached 0.01 m m ⁻¹ s ⁻¹ at 200 m slant range and decayed down to the order of 0.001 m m ⁻¹ s ⁻¹ at 1000 m slant range. Peak strain rates were initiated by the first arriving phases at 200 m slant range but by later arriving phases thereafter. Each time series represents the values measured at a single DAS channel located at the slant ranges indicated in the legend.	19
Figure 13.	Trace normalized strain rate as a function of time at multiple ranges for the helical (blue line) and straight (orange line) cables	19
Figure 14.	Trace normalized strain rate in the downhole sections of the straight fiber in the .06 Bypass as a function of time at various depths relative to the bottom of the borehole (0m)	20
Figure 15.	Spectral amplitude at individual DAS channels on the straight fiber at multiple slant ranges.	21
Figure 16.	Spectral amplitude at individual DAS channels on the straight fiber at multiple slant ranges prior to the explosion.	21
Figure 17. Tra	ice normalized DAS data overlain by the waveforms at multiple ranges in the surface sections of the straight cable. Waveform amplitudes are multiplied by a factor of 10 to make them visible on this figure	23
Figure 18.	Trace normalized DAS data overlain by the waveforms at multiple ranges in the surface sections of the straight cable in the borehole at 206 m slant range (left column) and 239 m slant range (right column). Waveform amplitudes are multiplied by a factor of 10 to make them visible on this figure. The depth convention for this figure is explained in Figure 14	23
Figure 19.	Trace normalized DAS data showing an example of an aftershock in the P-Main drift.	24
Figure 20	Trace normalized DAS image showing numerous aftershocks in a 45 second window recorded by fiber in the .06 Bypass drift	25
Figure 21	Trace normalized DAS image showing a single aftershock recorded by fiber in the .06 Bypass drift. Data from three separate channels are extracted and overlain as time series on top of the DAS image (black lines).	25
Figure 22	a) Histogram of aftershock activity for the 6-hour period following PE1-A. b) Aftershock histogram for 1-hour period following PE1-A.	26

Figures vii

1.0 Introduction

On 18 October 2023, a 16.3-ton TNT equivalent chemical explosion was detonated underground at the Nevada National Security Site (NNSS), generating a seismic event (Myers et al., 2024). This event, PE1-A, was the first in a series of chemical explosions named the Physics Experiment 1 (PE1) series conducted by the Low Yield Nuclear Monitoring Program (LYNM). The seismic wavefield generated in PE1-A was measured on a distributed acoustic sensing (DAS) array designed and installed to sense the seismic wavefields from all events in the PE1 series. This report documents the design and installation of that DAS sensing system in the P-Tunnel complex of the NNSS. It also discusses the acquisition of DAS data for PE1-A and the associated observations. Analyses of PE1-A observations will follow in peer reviewed literature.

2.0 DAS Exploration of Explosion Phenomenology

DAS is being developed as an experimental technology used for detailed observations of the space-time structure of seismic wavefields (e.g., Lindsey et al., 2020). DAS is a technology based on interferometry that involves sending a pulse of laser light down a fiber optic cable and then observing the difference between the expected and received signals. That difference occurs because of local strain or strain rate on the cable due to motion of the material surrounding the cable, such as ground motion when the cable is directly buried (e.g., Lindsey et al., 2020).

This technology is being developed for modern problems of seismic monitoring which are distinct from traditional single-point sensing because it is recognized that temporal variations and spatial irregularities in both the seismic wavefield and ambient environment contribute significantly to the event-generated pattern of surface ground motion. DAS offers dense, phased-array sensing capabilities with wide coverage, a high dynamic range, and dynamic and time-synchronized measurements along the entire sensing cable length. This class of methods is therefore well suited for characterizing complex surface motion patterns induced by a range of signal sources, from weak hammer hits to strong explosive-generated seismic waves. For explosion monitoring programs, this performance range may be particularly critical for characterizing and interpreting the surface motion from small explosions for which the density of single point sensors may seldom be large enough to sufficiently characterize the associated complexity in the wavefields.

DAS has been successfully used to characterize many aspects of chemical explosion phenomenology, including spall, wavefield evolution, surface response, and geologic effects on propagation (e.g., Abbott, 2019; Mellors et al., 2021; Porritt et al., 2022; Veins and Delbridge, 2024). It may also be a rich data set for exploring aspects of the transition, from seismic signal generation to propagation in chemical explosion experiment series—which have been difficult to understand from historic observations using arrays of single point sensors. For example, it can be difficult to understand if observed asymmetries in the seismic wavefield were generated at the seismic source or introduced during propagation through heterogenous geologic mediaboth of which may contribute significant scatter to seismic waveforms and must be separated to understand source processes alone (e.g., Strojkova et al., 2015). Furthermore, while these wavefield asymmetries may be damped in the low-frequency seismic component observable at teleseismic distances for large explosions, they may persist for proportionately more of the propagation path in seismic observations of both the low and high frequency components of small explosions in signals that are only observable at local or regional distances. Thus, measurements are sought of the explosion-generated seismic signal transition from generation to propagation in sufficient characterization at both high and low frequencies to enable source processes to be isolated in signals observed at the local to regional scale, and for which DAS is well suited. In particular, the high frequency (> 10 Hz) seismic behavior in 0.5 – 3.0 km range for chemical explosion experiments is currently not well characterized. Additionally, the 0.5 – 3.0 km range is the typical region over which there is a transition from generation to propagation dominated behavior that occurs for explosion experiments. Insight into that process and behavior may be possible from DAS measurements of chemical explosions, which has not been possible with seismic data from traditional seismic sensors.

3.0 DAS for the PE1 Series

3.1 Design

A new series of large-scale chemical explosions conducted by the LYNM program is contributing to this exploration of small-explosion seismology (Walter et al., 2023; Meyers et al., 2024). This series of explosive events will occur in the P-Tunnel complex at NNSS in southern Nevada (see Figure 1). The series of explosions will vary in magnitude and occur in multiple different drifts created in the tunnel generating a range of ground motions with a variation in source origin (Walter et al., 2023). Additionally, the motion will be induced in the predominate local geology of the P-tunnel complex which is vitric non-welded tuff with multiple geologic features at the meter to tens of meters scale, including subunits, faulting and fracturing, and variations in lithologic properties such as porosity, density, saturation, etc. (Bodmer et al., 2024).

For this series of explosions, the seismic signal will be recorded using DAS as a multichannel seismic array. The PE1 DAS installation was therefore designed to capture the range of possible signal strengths and incidence angles from a source with multiple locations in a geomaterial with meter- to tens-of-meter scale heterogeneity, within installation constraints of the site. This work builds on previous work by extending DAS observations to smaller explosive-scaled ranges, extending DAS observations to a new explosion scenario (an explosion from a horizontal tunnel rather than a vertical borehole), and measuring a source with co-located straight and helical fibers to compare performance and measuring on a smaller helical winding angle (e.g., Abbott, 2019).

This installation was also designed to examine the motion induced both by individual explosions and provide a data set from which all explosions in the series could be compared. This was achieved by installing DAS cables in two separate locations in the tunnel complex and by installing two sets of cables in each of those locations. To examine the motion of each individual explosion, DAS fiber was emplaced in the .06 Bypass drift which is the access drift nearest the drifts from which the explosions would be generated. Because of the orientation of the .06 Bypass drift (and therefore the fiber within that drift) with respect to the explosive sources, there is a large variation in incidence angles along the fibers which complicate a comparison of all the measured wavefields on this section of fiber. The variation in incidence angles is expected to be much smaller in the P-Main drift and that section of the installation was designed to support the comparison among all explosions in the series. For PE1-A, the first experiment in the series, the array provided measurements at a slant range of 27 m to 1123 m, with a gap of 85 m between segments (see Figure 1). The slant-range or range distance is defined here as the threedimensional distance between the sensor location and the center of the explosive and is used here in place of the more commonly used distance along fiber measurement to capture the explosive phenomenology observed at various radial distances.

While relatively smaller, the variation in incidence angles in P-Main, as well as the .06 Bypass, may still complicate the interpretation of the motion and so the array was designed with a combination of co-located straight and helical cables in both P-Main and the .06 Bypass drift to facilitate the comparison of signals across the array for each experiment and across the experiment series. DAS data exhibit sensitivity which is dependent on the angle of incidence of seismic energy with respect to the orientation of the fiber. In general, this results in enhanced sensitivity (maximum fiber strain) to the motion aligned with the axial direction of the fiber (motions that locally stretch or compress the fiber) and reduced sensitivity to motion perpendicular to the fiber (minimum fiber strain). The combination of both straight and helical

cables broadens the incidence angle range that the array is sensitive to for incoming seismic waves and thereby increases the sensitivity of the array to both P-waves that are more likely to produce parallel motions on the fiber and shear waves that are more likely to produce perpendicular motions on the fiber. Each cable was a tight-buffered tactical cable design and was selected to ensure installation durability in the operational tunnel environment. In one cable, an engineered Constellation® fiber had straight configuration, meaning the fiber was parallel with the fiberoptic cable core. In the other cable, the fiber had a helical configuration wherein an engineered Constellation® fiber was helically wound around the fiberoptic cable core at a calculated winding angle of 7.5 degrees. The optimal winding angle for maximizing measurements of P-waves and shear waves is 30 degrees (Kuvshinov, 2016). Due to experimental variances, the installed cable has a winding angle of 7.5 degrees.

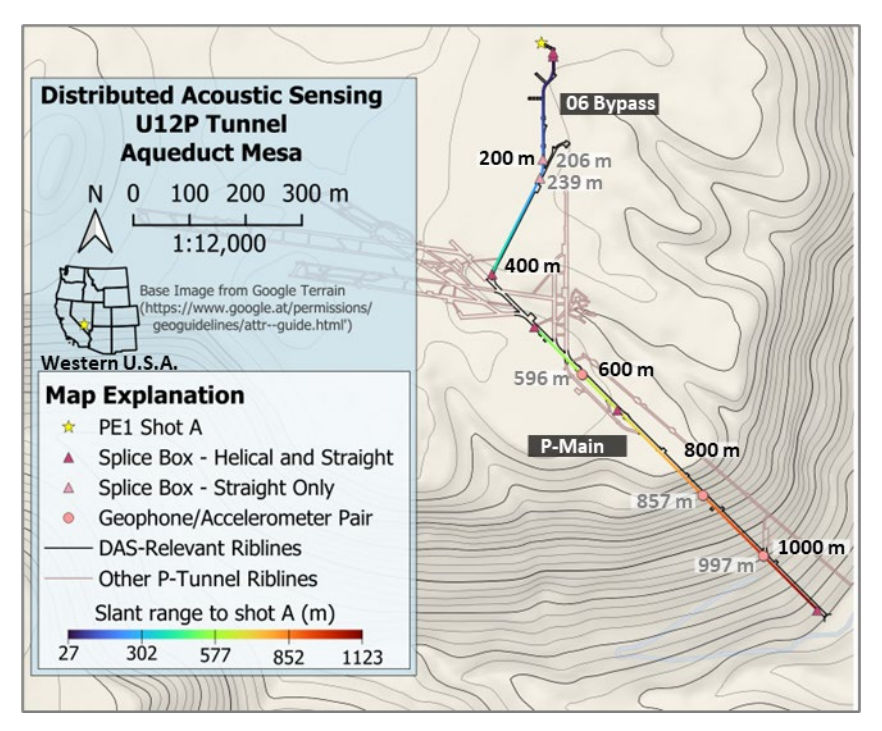


Figure 1. A map showing the DAS fiber installation that was used to record the PE1-A explosion in P-tunnel complex of the NNSS. Straight and helical DAS cables were installed in the P-Main and .06 Bypass drifts and shallowly buried in the tunnel floor from a scaled range of 27 m to 1123 m for PE1-A. The colormap represents the slant range to the center of the explosion for PE1-A, denoted with a yellow star. Locations where the cable was spliced are shown in triangles and co-located geophone and accelerometer pairs are shown in circles. A topographic map of Aqueduct Mesa underlays the tunnel map to indicate Aqueduct Mesa above the tunnel complex.

Additionally, due to the range of potentially important scales of geologic features in the test bed, a small gauge length and high sampling rate was desired due to the strong motion expected from the explosive phenomena. Both design requirements were achieved with Silixa's Constellation® fiber and Carina® interrogator unit, which enabled a maximum sampling rate of 100 kHz at a minimum gauge length of 2 m and provided the highest spatial and temporal sampling possible for capturing the strong expected motion induced by the explosion with the most fidelity and increased the maximum recoverable signal amplitude. The Carina® sensing system, which consists of both the interrogator unit and the Constellation® fibers, typically achieves a measurement performance comparable to the sensitivity of geophone systems.

3.2 Installation

The cables for this installation were installed in June 2022. The emplacement varied between the two sections of cable. In P-Main, the cables were emplaced in an existing trench filled with a concrete form that was built as a drainage trench for the tunnel. The form was approximately 25 cm deep, 10 cm wide at its base, and 15 cm wide at its top. The trench form was cleaned and prepared for emplacement by Mission Support Test Services (MSTS) with a 2.5-cm basal layer of fine sand, as shown in Figure 2.

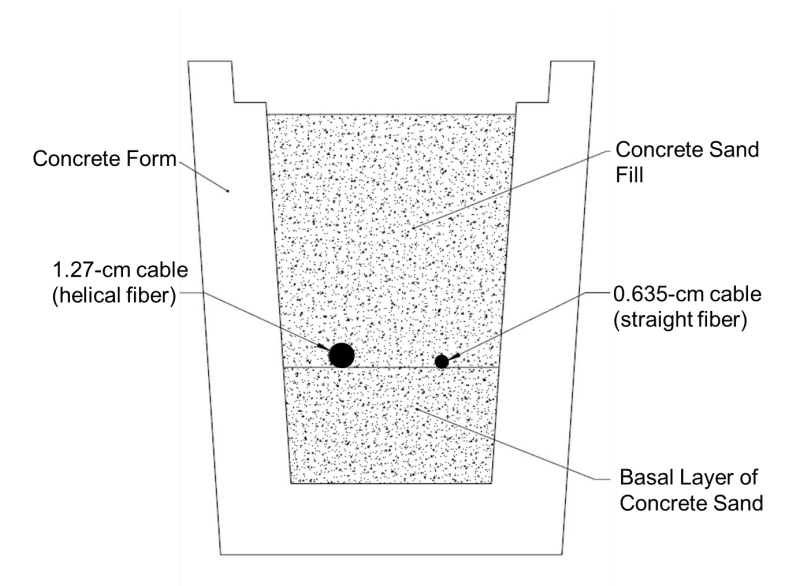


Figure 2. Cross-sectional schematic of cable placement in existing trench in P-Main.

Photographs of the emplacement process for the P-Main drift are shown in Figure 3. The reels of cable were loaded onto a rail car and driven down a rail through the center of the drift. The cables were pulled simultaneously off the reel by hand by MSTS electricians, taking care to never exceed the maximum bend radius of the cables, and laid on the floor of the tunnel. Once the full length of cables was cut off the reel, the cables were manually moved to the trench by the electricians and separated by approximately 7 cm in the trench. The trench forms were then filled with fine sand to couple the cable.

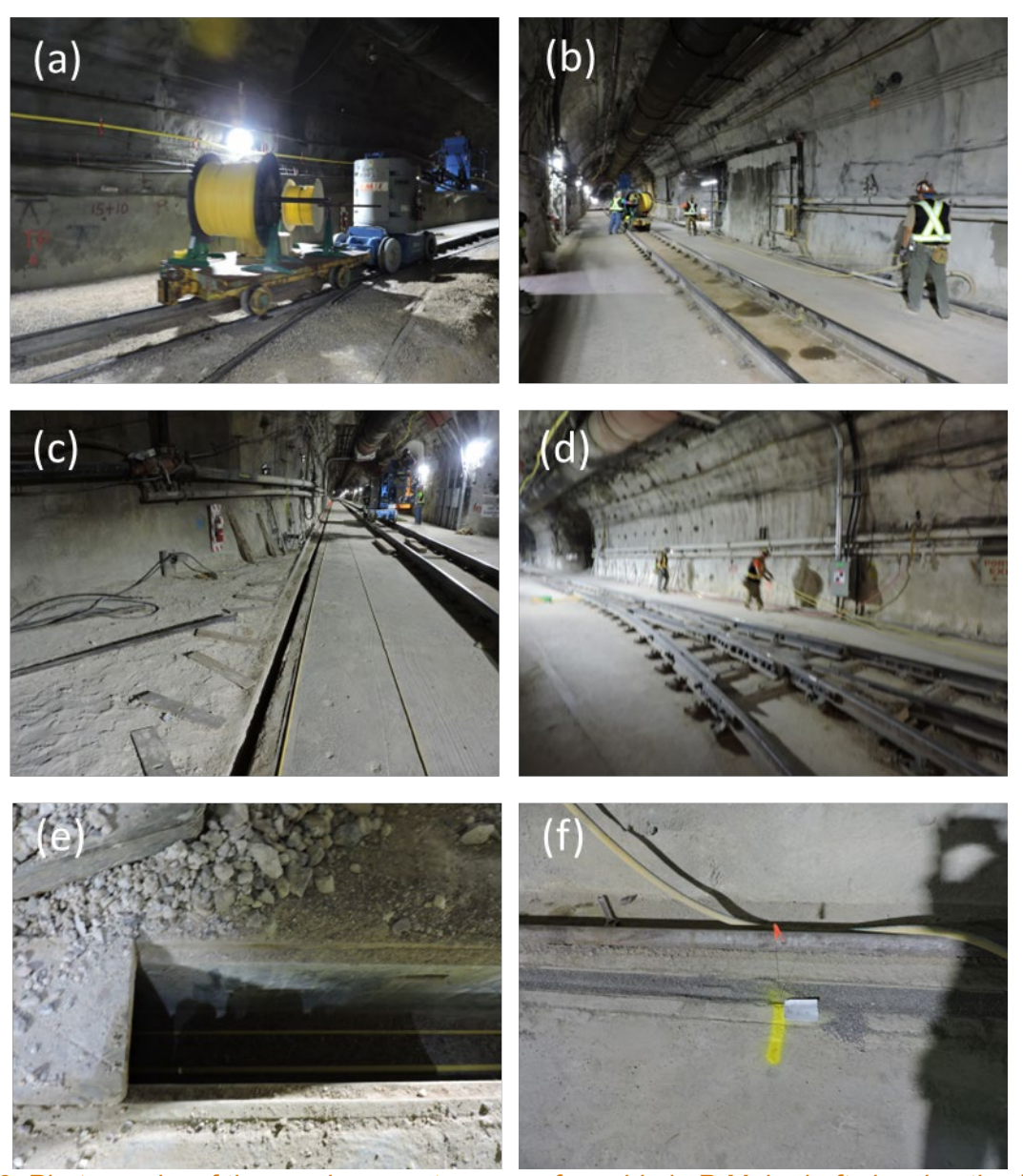


Figure 3. Photographs of the emplacement process for cable in P-Main draft showing the (a) yellow cable jackets of the fiber on the reels on rail car;, (b) staff pulling the cable off the reels; (c) laying the cable on the ground next to the trench; (d) laying the cable in the trench; (e) cables spaced within trench; and (f) trench filled with sand. Photos by K. Chojnicki.

Five sections of the P-Main emplacement deviated from this general emplacement procedure. In two sections of the trench at around 645 m and 717 m slant range, the trench went underneath existing steel rails for train tracks and the cable was manually fed under the rails by MSTS (see Figure 4). To minimize the length of cable fed under rails, the cable was cut and spliced together at a slant range of approximately 667 m.

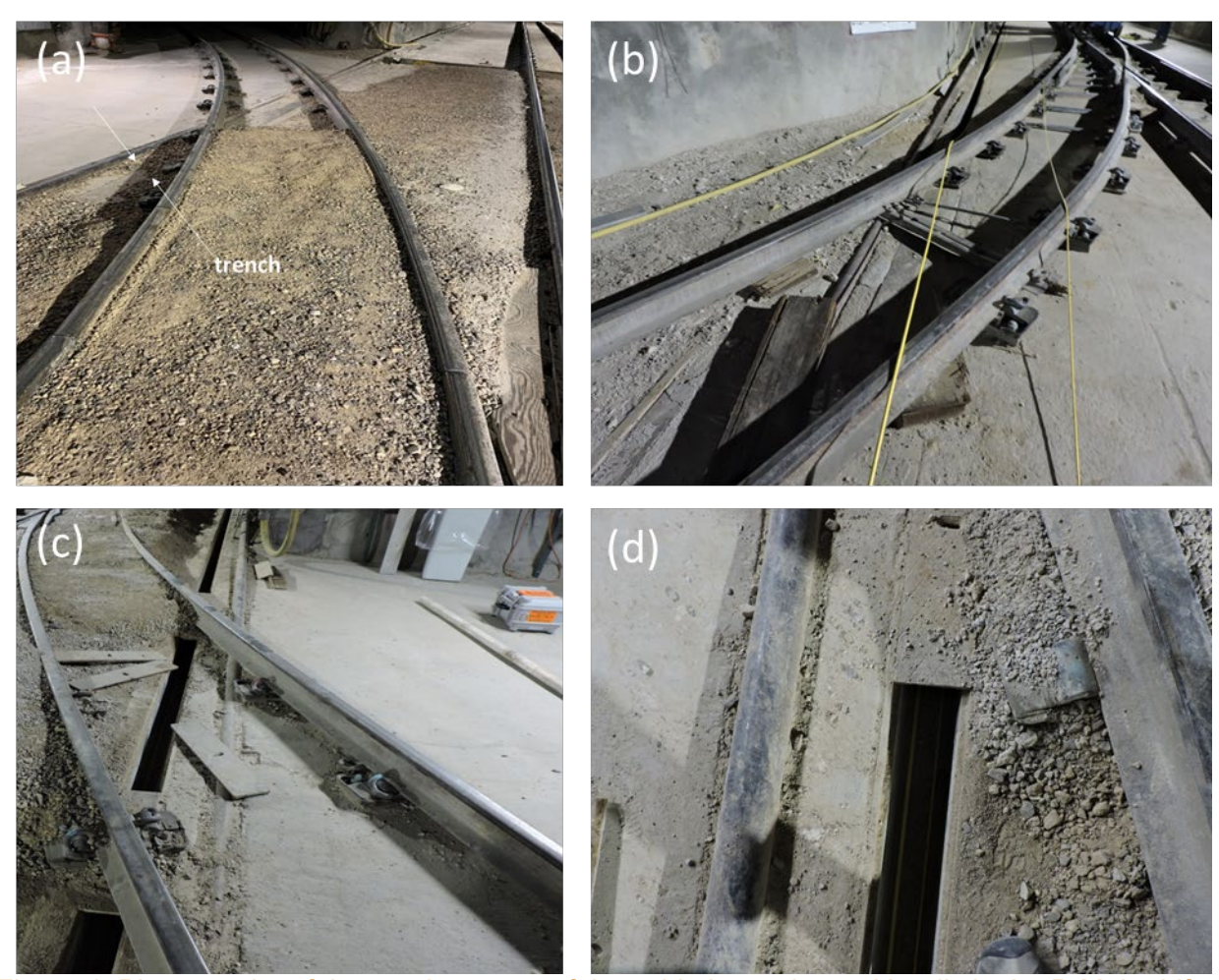


Figure 4. Photographs of the emplacement of the cable in sections with rails in the P-Main drift showing (a) the pre-existing trench in the P-Main drift that was leveraged for this installation; (b) the cables laid across the rails prior to being routed under the rails; (c) the areas the rails cross the trench; and (d) the cables once they were installed in the trench. Photos by K. Chojnicki.

The trench was discontinuous in three sections because of infrastructure at around 585 m, 685 m, and 755 m slant range. In these places the fiber cables were routed out of the trench by plastic cable guides, laid into plastic pan conduit to traverse the sections of existing infrastructure, and then routed back into the trench with cable guides. The guides and pan conduit trays were filled with sand and then sandbags were placed on top of the closed trays to couple them to the infrastructure on the tunnel floor. Photographs of this process are shown in Figure 5.

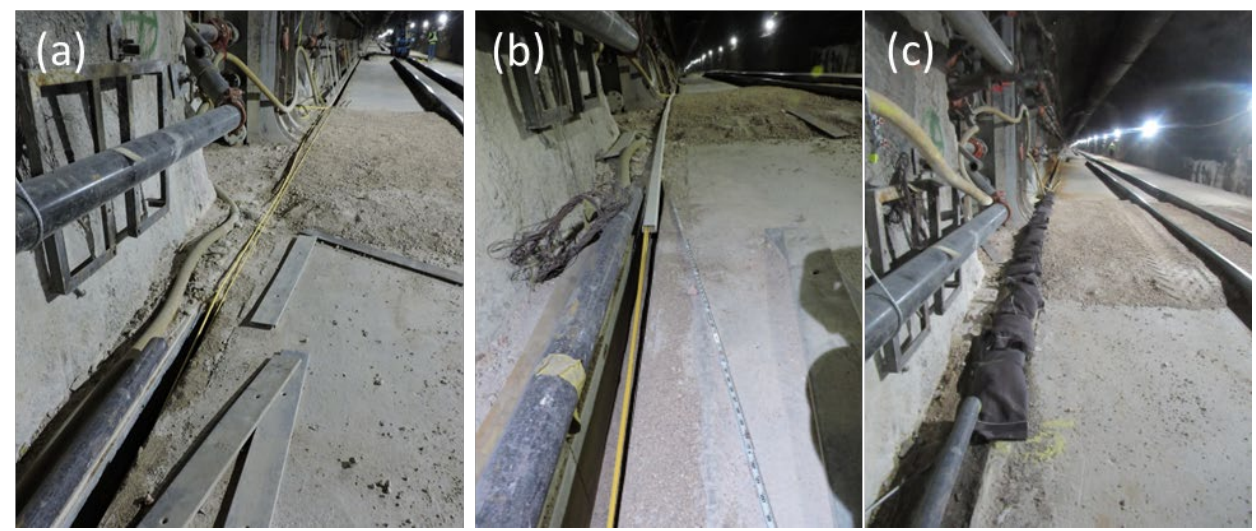


Figure 5. Photographs showing the areas where cables in P-Main were routed; (a) out of a trench over an existing piece of infrastructure, and then down back into the trench; (b) the panduit (white material) that was installed to guide the cable; and (c) sandbags placed on top of the conduit. Photos by K. Chojnicki.

The sensing fibers were spliced to communications cables at the splice box at 1123 m slant range which were routed outside the tunnel and to a shipping crate that served as the instrument operations room where the interrogators, computers, and RAID drives were located during the acquisition.

The emplacement in the .06 Bypass involved MSTS digging a new trench in the fill composing the drift floor near the left rib of the drift to a depth of at least 20 cm and a width of at least 15 cm. A 2.5 cm bed of sand was placed at the bottom of the trench to line it. The linear and helical cables were simultaneously pulled off reels on rail cars that were driven down the tunnel, as shown in the photographs in Figure 6. The cables were laid directly into the trench or routed under existing infrastructure, such as cable conduits, that crossed the trench. An example is shown in the photographs in Figure 7. The trench was then filled with approximately 15 cm of sand to couple the cable.



Figure 6. Photographs of the emplacement in the .06 Bypass drifts showing (a) cable reels on rail cars, (b) staff pulling the cable off the reel, (c) guiding the cable into the trench, and (d) the final placement of the cable in the trench. Photos by K. Chojnicki.



Figure 7. Photographs showing an example of cables being routed around existing infrastructure in the tunnel by (a) digging a trench below this pre-existing cable conduit, and then (b, c, d) routing the cable under the conduit(s). Photos by K. Chojnicki.

Additionally, the straight cable in the .06 Bypass was also installed down two boreholes at 206 m slant and 239 m slant range, each of which was approximately 9 m deep and located in the center of the drift. A separate loop of cable was emplaced downhole and the apex of the loop had a cable guide component designed and manufactured by Silixa, LTD to minimize the chances of exceeding the cable bend radius during the installation downhole (see Figure 8). At the top of each borehole, the cable was fed into an air-filled vault and then routed from the vault at center of the drift to the left edge of the drift where the trench for the DAS cables was located and then spliced by Silixa, LTD to the surface sections of cable in the cable trench. The boreholes were then filled with grout to couple the cable.



Figure 8. Photographs showing the installation process of the cable down boreholes, including (a) the cable and the apex loop cable guide secured to the cable guide; (b) the cable guide being inserted downhole; (c) the cable completely installed downhole; and (d) the completion of grout in the borehole. Photos by PE1 Experiment Team.

Both the straight and helical cables in the .06 Bypass were spliced to communications cables at the splice box near 400 m slant range. The communications cables were then routed outside the tunnel and to a shipping crate which served as the instrument operations room where the interrogators, computers, and RAID drives were located during the acquisition.

The physical locations along the fiber sensing arrays were mapped using a tap-test procedure. In this procedure, a signal was generated, such as hitting the ground next to the cable with a hammer, and the physical location of the location the hammer hit was then surveyed. That signal was then identified in the data and the peak picked manually to determine the single channel, or distance along fiber, at which that signal appeared. That channel was then mapped to that location in space. Both the locations of the tap tests and the number of locations were chosen to optimize spatial control in areas where the cable changed direction or where the features in the tunnel environment, such as existing infrastructure, which could contribute vibrations in the data. Tap-testing in the P-Main drift occurred in August 2022 with 20 locations mapped.

As there was a lot of complexity in the tunnel geometry and existing infrastructure in the .06 Bypass, 56 locations were tapped in October 2022. The tap-test locations form the control points for the mapping of the points in space to distance along the hundreds of meters of fiber and an interpolation procedure was used to map the channels in between the control points. Overall, this procedure resulted in a location uncertainty of less than the 1-m channel spacing for most interpolated points, with a few exceptions for areas in the .06 Bypass near where the downhole cable sections are spliced to the direct-buried cable sections.

The cables are also co-located with three geophone and accelerometer pairs for amplitude comparisons at 596 m, 857 m and 997 m slant range. Example photographs of this installation is shown in Figure 9. The geophones and accelerometers were emplaced in the sand at the top of the trench form and each pair was spaced by 2 m—the equivalent of one DAS gauge length. The geophone and accelerometer transverse horizontal components were aligned to the axis of the DAS cable. The six geophones (Geospace Technologies GS-11d) had natural frequencies of 4.5 Hz and the six accelerometers (Kinemetrics Episensor 2) were set to a 4 g response. Both geophones and accelerometers were connected to RefTek digitizers that were powered by a supply unit charged by line power in the tunnel. The geophones were installed in December 2022 and the accelerometers were installed in July of 2022. In August of 2022, the geophones and accelerometer data were telemetered to a server maintained by the University of Nevada, Reno (UNR). Telemetering supported real-time health assessments and UNR provides archived access to the data.







Figure 9. Photographs showing the (a) co-located geophone and accelerometer installations; (b) an example geophone and accelerometer; and (c) an example digitizer and the power source. Photos by K. Chojnicki.

4.0 DAS Data for PE1-A

4.1 Acquisition

On 18 October 2023 at 8:15:00 am local time (15:15:00.00 GMT), a 16.3-ton TNT equivalent chemical explosion was detonated underground at the NNSS, generating seismic waves that were recorded on the DAS array illustrated in Figure 1 (for more information see Meyers et al., 2024). Multiple acquisition settings were used in this experiment to optimize recording of early and late time behavior, targeting the first arriving phases at early times and aftershocks at later times. This paper focuses on the early time behavior but does overview some late time behavior. For the early time behavior, Carina interrogators were used with the Constellation® fibers to enable collection by Silixa, LTD of a gauge length of 2-m and a sampling frequency of 100 kHz in the .06 Bypass, and a sampling frequency of 80 kHz in P-Main for 15 minutes after the explosion. These sampling times are summarized in Table 1. There is a nominal 5-minute break between the early and late time settings, during which the acquisition was stopped, the settings were changed on the equipment, and acquisition resumed at the late time settings. Four interrogators were used to record the data, one for each cable section (the straight cable in P-Main, the helical cable in P-Main, the straight cable in the .06 Bypass, and the helical cable in the .06 bypass). The geophones and accelerometers recorded at 1 kHz and access to the realtime data was limited to select individuals during the experiment.

Table 1 Summary of DAS Sample Rates for PE1-A

DAS Cable Section	Early Time Sample Rates	Late Time Sample Rates
	t - 5 minutes - t + 15 minutes	t + 15 minutes – t + 24 hours
Straight, .06 Bypass	100 kHz	1 kHz
Helical, .06 Bypass	100 kHz	1 kHz
Straight, P-Main	80 kHz	1 kHz
Helical, P-Main	80 kHz	1 kHz

4.2 Processing

The DAS data were filtered at 200 Hz using the lowpass filter function in Matlab with a filter value of 0.004 for the .06 Bypass (a range of 27 m to 420 m) and 0.005 for P-Main (range of 505 m to 1123 m) which is 200 Hz/Nyquist frequency for each section. The Fourier spectra were computed for 1.5 seconds using a discrete Fourier transform. A sampling frequency of 100 kHz and Nyquist frequency of 50 kHz was used for the .06 Bypass (slant ranges 27 m to 420 m) and a sampling frequency of 80 kHz and Nyquist frequency of 40 kHz for P-Main (slant ranges 505 m to 1123 m). Frequency content for many of the channels in the data (e.g., at a range of ~256 m, ~645 m, 667 m, ~685 m, ~717 m, ~755 m) reflect effects of existing infrastructure on the data which result in noisy data at those locations.

4.3 Signal Confirmation

The first arrival from the explosion temporarily saturated both cables at ranges between 27 m to 186 m, but strain rate was successfully measured on both cables for the remainder of the array. The strain rate waveforms measured for the entire array are shown in Figure 10a for the first 1.5 seconds after the explosion. Each waveform, or trace, is normalized by its peak absolute value in that time window to enable a visualization of the trends across the array despite the orders of magnitude variation in amplitude. Figure 10a illustrates that timing of the first arrival was successfully measured across the entire array as shown by the moveout of the first arriving phase in the southeast trending linear feature on this plot. The first arrival reached the start of the array, at a range of 27 m at 0.01 s and reached the end of the array, at a range of 1123 m at 0.5 s. The noise on the channels with existing infrastructure does not reduce the coherence of the wavefields across those features.

From a range of 186 m to 420 m, the first arrival traveled with an apparent velocity of 2640 m s-1, according to the moveout on the straight DAS fiber in the .06 Bypass. From a range of 505 m to 1123 m the apparent velocity of the first arrival decreased to 2470 m s-1 according to the moveout on the straight DAS fiber in P-main. Once the first arrival reaches the end of the array, waves traveling back toward the interior of the tunnel are also visible in Figure 10a as the southwest trending features starting near a range of 1123 m and reach back to a range of 600 m. This results in a complex wavefield between ~850 m to 1123 m slant range, wherein waves arriving from the source are met by waves reflected from beyond the end of the array.

The frequency content of the DAS data as a function of distance is shown in Figure 10a. The saturated section of the data appears as a broadband signal from a range of 27 m to 186 m. At a range of 186 m, the frequency content for the first arriving phase started at a peak of around 200 Hz and then attenuated to a peak of around 50 Hz at a range of 1123 m. Using the apparent velocities listed above, the computed apparent seismic wavelengths were about 20 m across the array; starting from 13 m at a range of 186 m, increasing to about 17 m at a range of 420 m, and to about 25 m at a range of 1123 m.

While the frequency content generally reduces monotonically across the array, there is a slight increase in peak frequency content from 800 m to 900 m slant range along with a decrease in spectral amplitude. Similarly, while the spectral amplitude appears to decrease monotonically across the array, there is an apparent increase from a range of 1000 m to 1123 m. It is unclear what causes the variations in the trends in frequency values or spectral amplitudes between 800 m and 1000 m, but it is thought to be related to the combination of waves simultaneously traveling toward and away from the explosive source in that region of the array as shown in Figure 10a. The transition from higher (hundreds of Hz) to lower (tens of Hz) frequencies is directly observable in the DAS strain-rate records at the meter scale over this slant range.

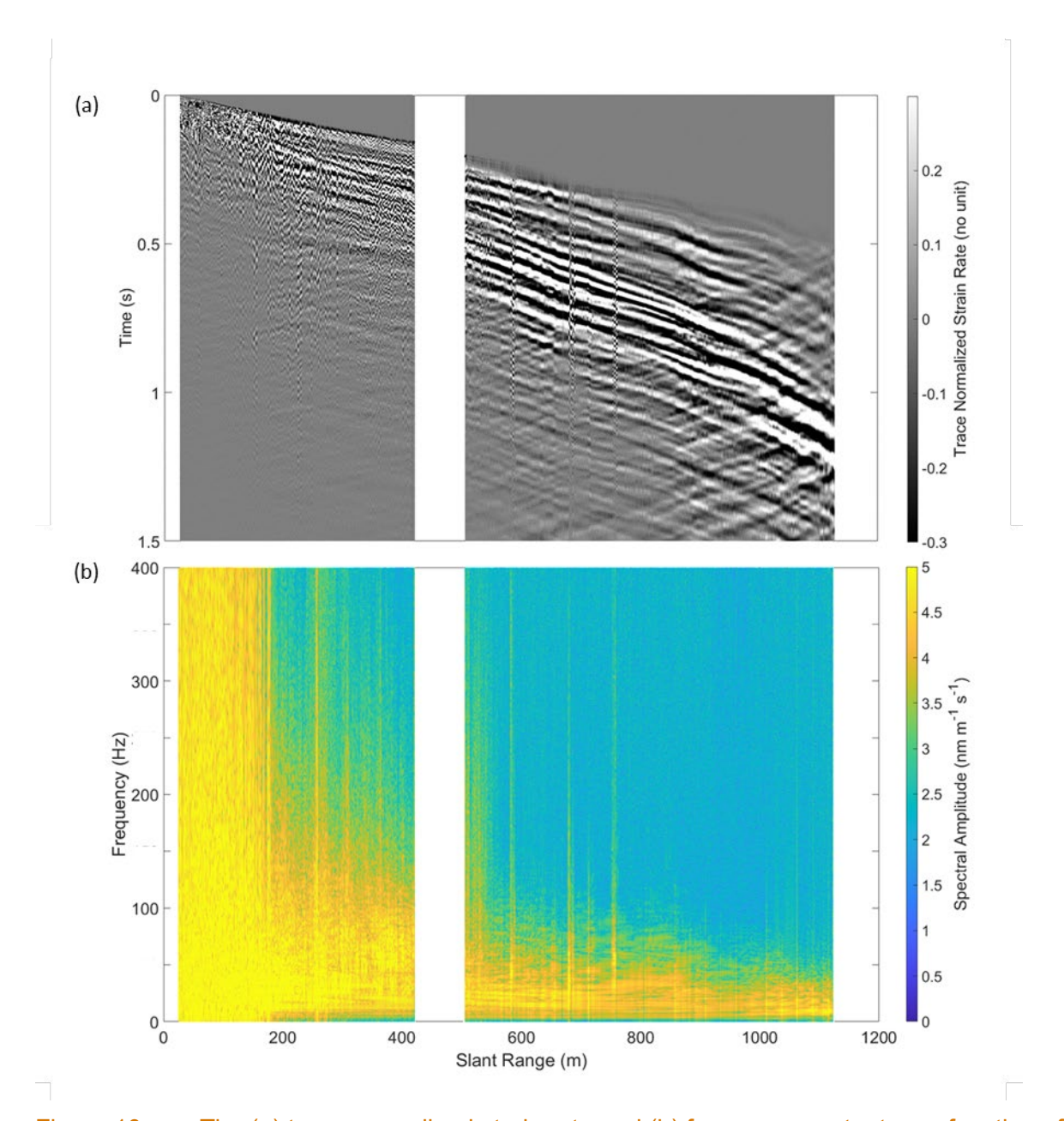


Figure 10. The (a) trace normalized strain rate and (b) frequency content as a function of slant range for the straight DAS cable in the first 1.5 seconds after the explosion. The data are low pass filtered at 200 Hz. The data were saturated from 27 m – 186 m slant range as indicated by the incoherent phase and broad-band frequency response in that region. Areas with known infrastructure contribute noise around 256 m, 585 m, 645 m, 667 m, 685 m, 717 m, and 755 m slant range (see text for more information).

4.4 System Performance

To further investigate the magnitude of the DAS strain rate amplitudes in relation to the velocity and acceleration measured on co-located geophones and accelerometers, the measured strain rate in individual channels in the straight fiber in P-Main were compared to calculations of strain rate from the co-located geophone and accelerometer pairs, as shown in Figure 11. Amplitudes of strain rates computed from co-located geophones spaced one gauge length apart (2 m) compare well with the DAS measured strain rates on the straight fiber in P-Main for two of the three pairs, at ranges of 857 and 997 m. The strain rate, $\dot{\epsilon}$, was calculated from the geophones as the change in velocity, V, between the geophones in a pair and divided by the spatial distance between the geophones in the pair, or

$$\dot{\epsilon}_{geophone} = \frac{V_2 - V_1}{x_2 - x_1},\tag{1}$$

where x is the location of a geophone in the pair. Similarly, amplitudes of strain rates computed from co-located accelerometers spaced one gauge length apart (2 m) compare well with both the DAS measured strain rates and the strain rates computed from the geophone pairs for two of the three pairs, at ranges of 857 and 997 m. Strain rates were computed from the accelerometers in a pair using the following expression:

$$\dot{\epsilon}_{accelerometer} = \frac{\int a_2 dt - \int a_1 dt}{x_2 - x_1},\tag{2}$$

where a is the acceleration. The source of the variation between DAS-measured and geophoneand accelerometer-computed strain rates at the pair at a range of 596 m is under investigation. The relative agreement between the measured and calculated amplitudes on the DAS and accelerometers and geophone pairs at ranges of 857 and 997 m suggest the DAS fiber faithfully recorded the ground motion amplitudes in this section of the fiber emplacement and supports the conclusion that the Carina system was able to achieve DAS measurements at the sensitivity of the geophones for this installation.

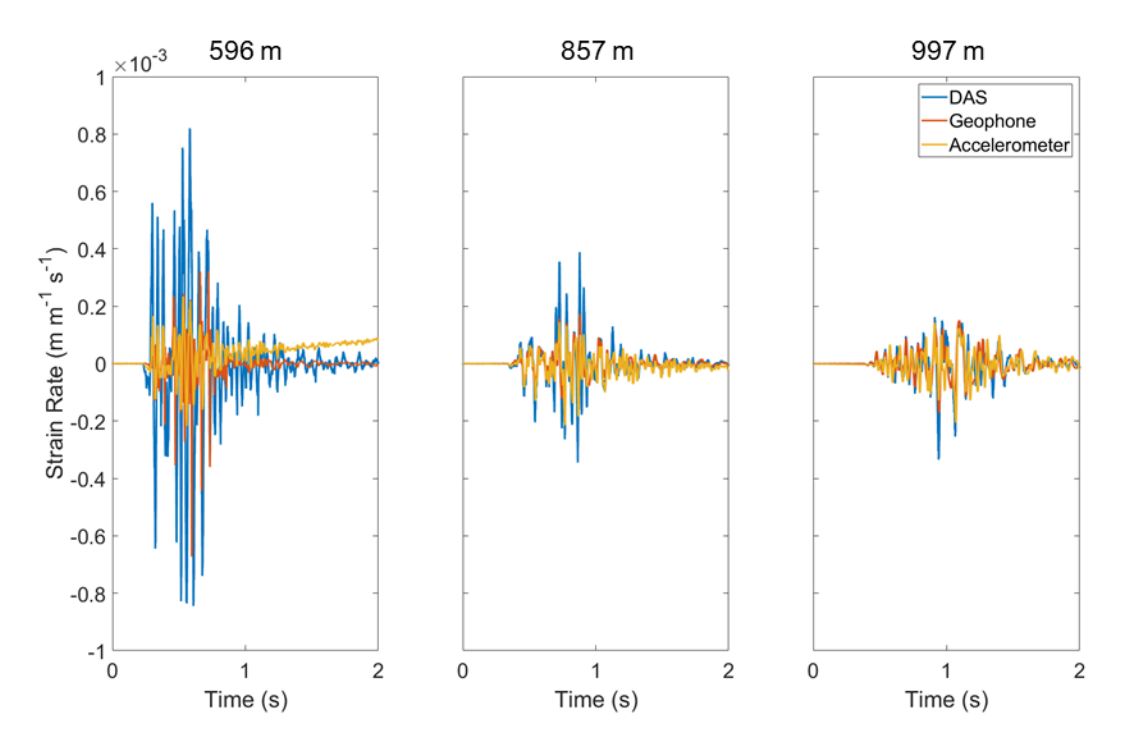


Figure 11. Strain rate as a function of time measured from DAS (blue line) and computed from the geophone (orange line) and accelerometer (gold line) pairs at 596 m, 857 m, and 997 m slant range.

4.5 Time Series

The strain rate measured on the straight DAS cable at single channels located at various distances from the center of the explosion, or slant ranges, for PE1-A are shown in Figure 12. The peak strain rate of the first arrival at a range of 200 m was -2.0x10⁶ nm m⁻¹ s⁻¹ which reduced to 7.9x10³ nm m⁻¹ s⁻¹ at a range of 1000 m. Peak strain rates for first arrivals at a range of 200 m were about 9× the peak strain rate values measured at a range of 400 m, 32× the peak value at 600 m, 145× the value at 800 m and 2024× the peak value measured at a range of 1000 m. This suggests the peak strain rates for first arrivals reduced approximately an order of magnitude every 200 m slant range up to 1000 m slant range. Peak strain rates were initiated by the first arriving phases at a range of 200 m but by later arriving phases thereafter.

Trace-normalized DAS waveforms at individual channels on the helical and straight cables at various slant ranges are shown in Figure 13. Overall, the response of the 7.5-degree helical cable is very similar to the straight cable with correlation coefficients above 0.97 between the waveforms at the same range except at a range of 800 m where the coefficient reduces to 0.87. The high correlation coefficients for the signals on individual channels at the same mapped locations in the straight and helical cables confirms the channel mapping uncertainty is less than 1 m, at least at these locations. If the uncertainty was greater, it is unlikely the individual channels would have correlated so well. The correlation coefficient between the helical and straight waveforms at channels nearby the 800 m slant range were investigated and determined to be less than 0.87, indicating the lower correlation value does not reflect a misalignment with the channel selection or mapping for that range. This variation may represent differences in the measured waveforms on the straight and helical cables and will be investigated by future work.

As the wavefield moves from a range of 200 m to 1000 m the trace-normalized first-arrival peak amplitudes decrease, the trace-normalized later-arrival peak amplitudes increase, and the width of the trace-normalized peaks increase. Additionally, at a range of 200 m the maximum amplitudes used in the normalization occur in the first arrivals as indicated by the timing of where the normalized strain rate has a value of 1. However, by a range of 400 m the later phases dominate the maximum amplitudes as indicated by the later times where the normalized strain rate has a value of 1, and they dominate thereafter.

The waveforms of the trace-normalized strain rates are shown in Figure 14 for the sections of straight fiber installed downhole in the .06 Bypass in the borehole at a range of 206 m (left side) and 239 m (right side). Waveforms recorded at multiple depths are shown for each downhole section in each borehole and the waveform at the bottom of each borehole is shown at 0 m as shown schematically in Figure 14. In this figure, depth is meters rather than slant range. The waveforms in individual channels at similar depths in both the down-going and upgoing section of the loops of cable (e.g., -4 m and 4 m) in both boreholes have correlation coefficients above 0.99, indicating both sides of the cable loop recorded the same signal at the same depth in each borehole. If different channels are chosen for the correlation, the coefficient decreases. The high correlation coefficients for the signals on individual channels at the same mapped locations in the upgoing and down-going straight cables again confirms the channel mapping uncertainty is less than 1 m, at least at these locations. If the uncertainty was greater, it is unlikely the individual channels would have correlated so well.

There are some variations in the trace-normalized waveforms with depth. The first arrivals in the borehole at a range of 206 m (left side) vary in relative amplitude with depth with the greatest amplitudes observed close to the top of the borehole. In contrast, at 239 m slant range the amplitudes of the first arrivals at the top of the borehole were the smallest, and the amplitudes at depths of 4 m in the up or down-going sections were similar to the amplitude at the bottom of the borehole at 0 m. The opposite trend in the variation in first-arrival trace-normalized amplitude with depth may be related to variations in the behavior of the wavefield at each location and/or it's possible there could be some local variations in the installation and/or well completions with depth.

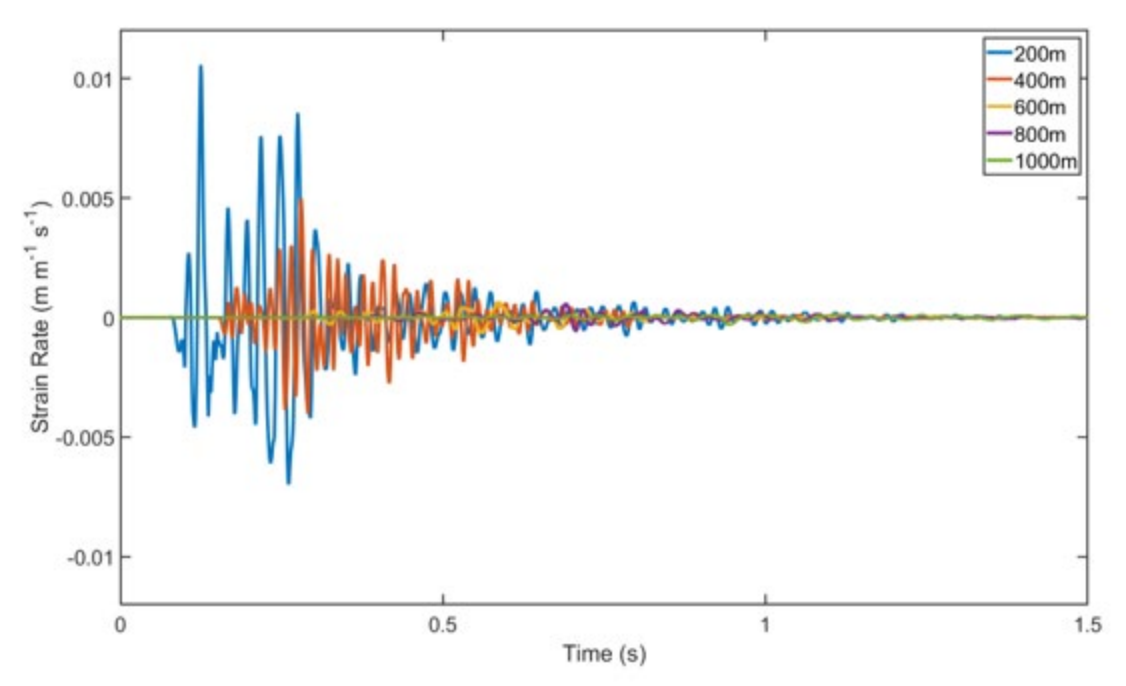


Figure 12. Peak strain rates induced on the cable from the detonation of PE1-A reached 0.01 m m⁻¹ s⁻¹ at 200 m slant range and decayed down to the order of 0.001 m m⁻¹ s⁻¹ at 1000 m slant range. Peak strain rates were initiated by the first arriving phases at 200 m slant range but by later arriving phases thereafter. Each time series represents the values measured at a single DAS channel located at the slant ranges indicated in the legend.

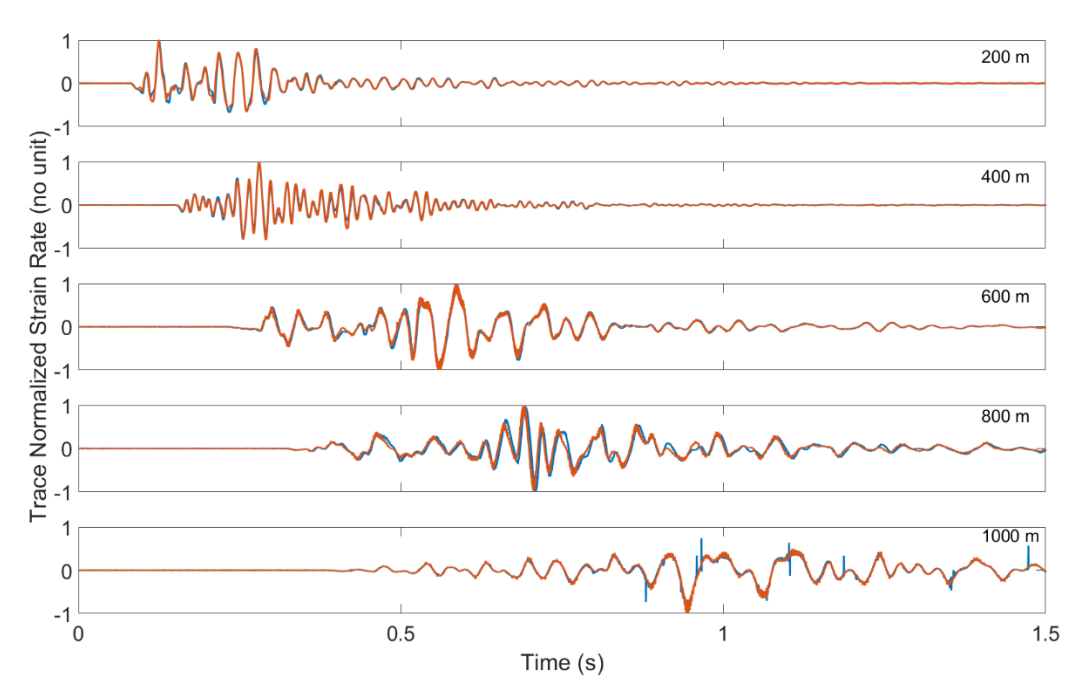


Figure 13. Trace normalized strain rate as a function of time at multiple ranges for the helical (blue line) and straight (orange line) cables.

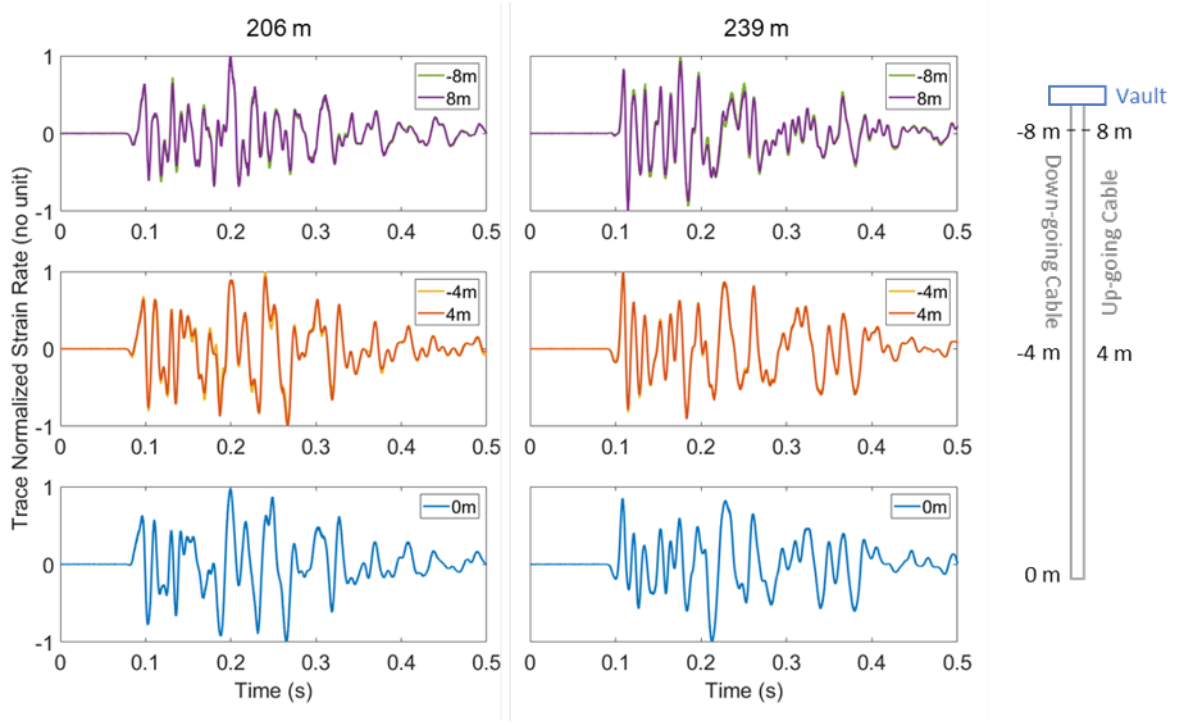


Figure 14. Trace normalized strain rate in the downhole sections of the straight fiber in the .06 Bypass as a function of time at various depths relative to the bottom of the borehole (0m).

4.6 Spectral Amplitude

The spectral amplitudes for multiple locations are shown in Figure 15 for individual DAS channels. In general, the spectral amplitudes at each distance increase in frequency, reach a peak, and then decrease in frequency before transitioning to a flatter trend at high frequencies. For PE1-A, the spectral amplitude peak reached 40.1 Hz at a range of 200 m, increased to around 61.8 Hz at 400 m, and then decreased from 16.5 Hz at 600 m to 10.4 Hz at a range of 1000 m. For ranges of 200 m and 400 m, the frequency coinciding with the spectral amplitude peak coincides with the corner frequency. However, for ranges of 600 m, 800 m, and 1000 m the corner frequency occurred after the spectral amplitude peaked and was 24.4 Hz, 33.5 Hz, and 24.4 Hz, respectively. The starting frequency value at which the spectral amplitude changes to a frequency-independent trend monotonically decreases with distance starting at 632 Hz for a range of 200 m, decreasing to 301 Hz for 400 m, 120 Hz for 600 m, 103 Hz for 800 m, and 83 Hz at a range of 1000 m. The spectral amplitudes for those same locations prior to the explosion are shown in Figure 16 for comparison.

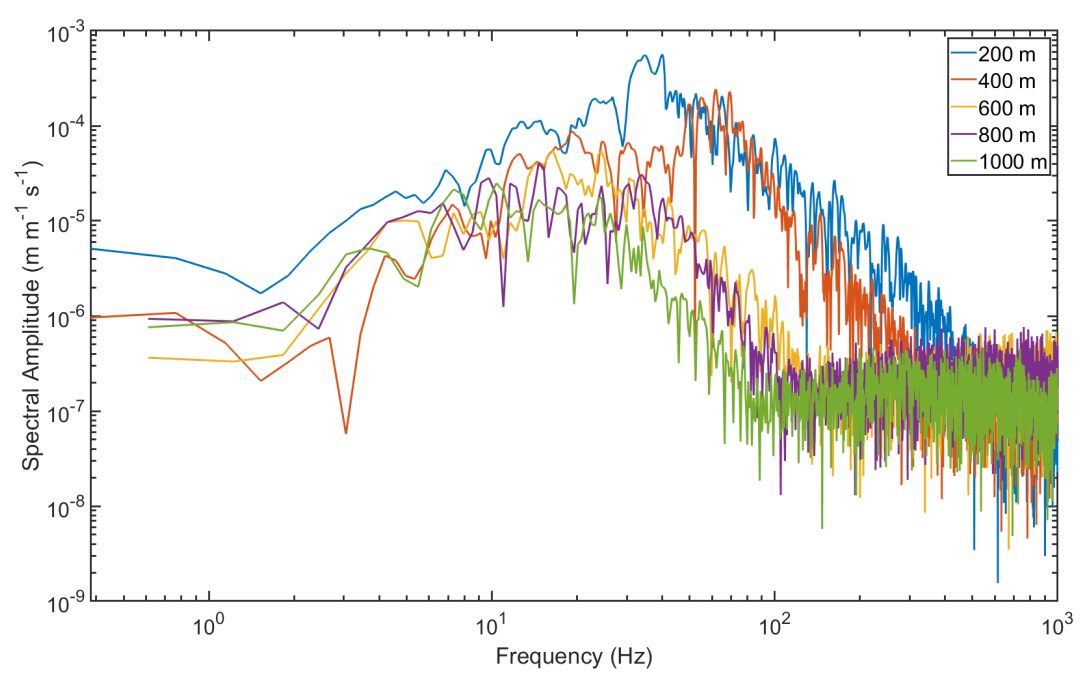


Figure 15. Spectral amplitude at individual DAS channels on the straight fiber at multiple slant ranges.

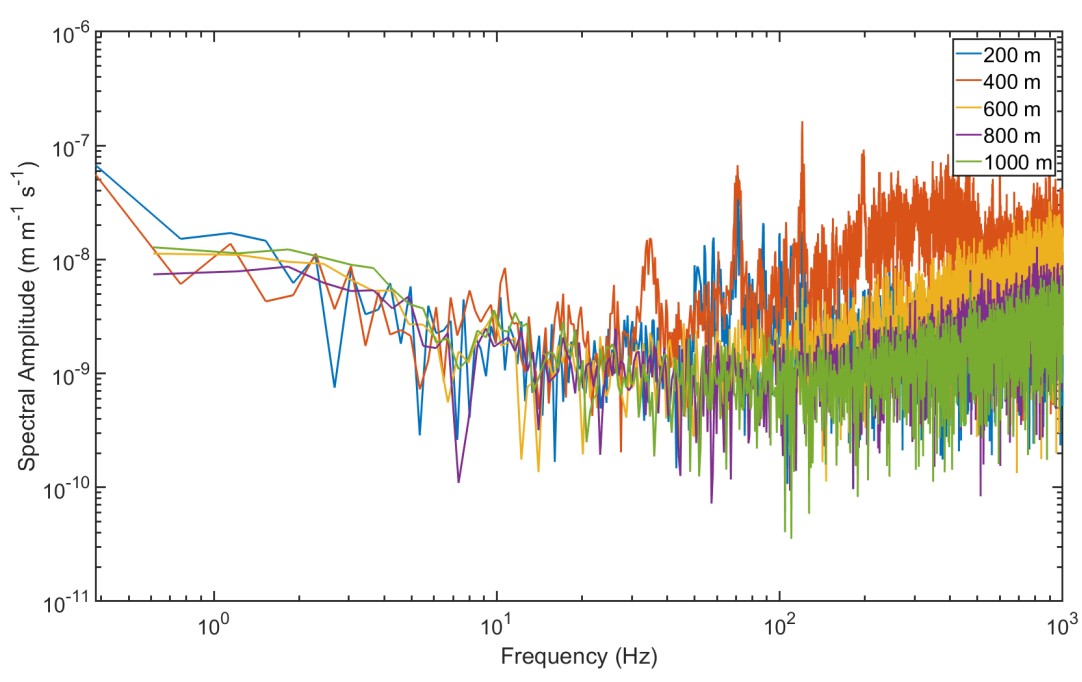


Figure 16. Spectral amplitude at individual DAS channels on the straight fiber at multiple slant ranges prior to the explosion.

5.0 DAS Exploration of PE1-A Explosion Phenomenology

A comparison of the individual waveforms from single DAS traces with the DAS images that include all traces provides context for interpreting features in the single traces, including identification of the phases responsible for the first arrival. An overlay of the waveforms on the raw DAS images in Figure 17 reveals that the peaks normally picked as the first arrival by analyzing individual waveforms alone were consistently associated with the same phase for slant ranges up to 400 m but were not associated with the same phases thereafter as the first arrival picks at 600 m, 800 m, and 1000 m slant each correspond with a different phase. This result suggests that for situations where the first arrival has a sharp onset that it may be reasonably assumed that the same phase likely comprises the first arriving phase, thus first arrivals picked on the waveform alone will represent the motion generated by the same phase as it propagates. However, once the first arrival transitions to something with an emergent onset, that assumption may no longer be reasonable and first arrivals picked on the waveform alone may not represent the motion generated by the same phase; instead it represents scattered energy from a refracted arrival. This transition from a sharp to emergent onsite of the first arriving phase occurred somewhere between 400 m and 505 m slant range for PE1-A. Without the context provided by DAS, it would be difficult to understand if first picks on traditional or single-point sensors would represent the motion of one phase and that could lead to a source of interstation variability and variance between observed and modeled values of the explosion phenomenology.

Traces for individual channels in the downhole sections of the straight cable in the .06 Bypass are shown in Figure 18. The first arrivals picked on the waveforms from all depths in the borehole at 239 m slant range would correspond with the same phase. This result is consistent with the results from the surface fiber which indicated a sharp onset to the first arriving phase until 400 m. In contrast, there is some apparent variation in the first arriving phase in the borehole at 206 m which seems to not have a coherent first arriving phase at all depths, with a negative phase at the top of the borehole and a positive phase at the bottom. There seems to be a mix of coherent and incoherent later arrivals in the borehole. While it is unknown what might be responsible for this variation, it may be related to emplacement differences with depth in borehole which could include the vertical position of the fiber in the well (which may change the relative incidence angle of the arriving waves) and/or local changes in properties of the grout completion that was used in the borehole.

The general trend in the spectral amplitudes from DAS at 1.1 km in PE1-A was consistent with the general trend in the displacement amplitude spectra observed at 4 km and 40 km for the NPE (Smith, 1994), which was also a tamped chemical explosion in a tunnel at the NNSS. The function of the general spectral amplitude trend may be a characteristic feature of the local-scale seismic wavefield for this type of explosion.

Additionally, there was an evolution of that spectra function from 0.2 to 1.1 km which was resolvable at the meter-scale with the DAS data in PE1-A. The processes contributing to that evolution will be the subject of future work and will hopefully shed light on the transition of that spectra from domination by source to propagation processes as evidenced by seismic observations. A comparison of these spectra with future experiments in the PE1 series may also shed light on how that transition may be different for different explosion source-types and better understand the factors which may govern the general spectral amplitude trends.

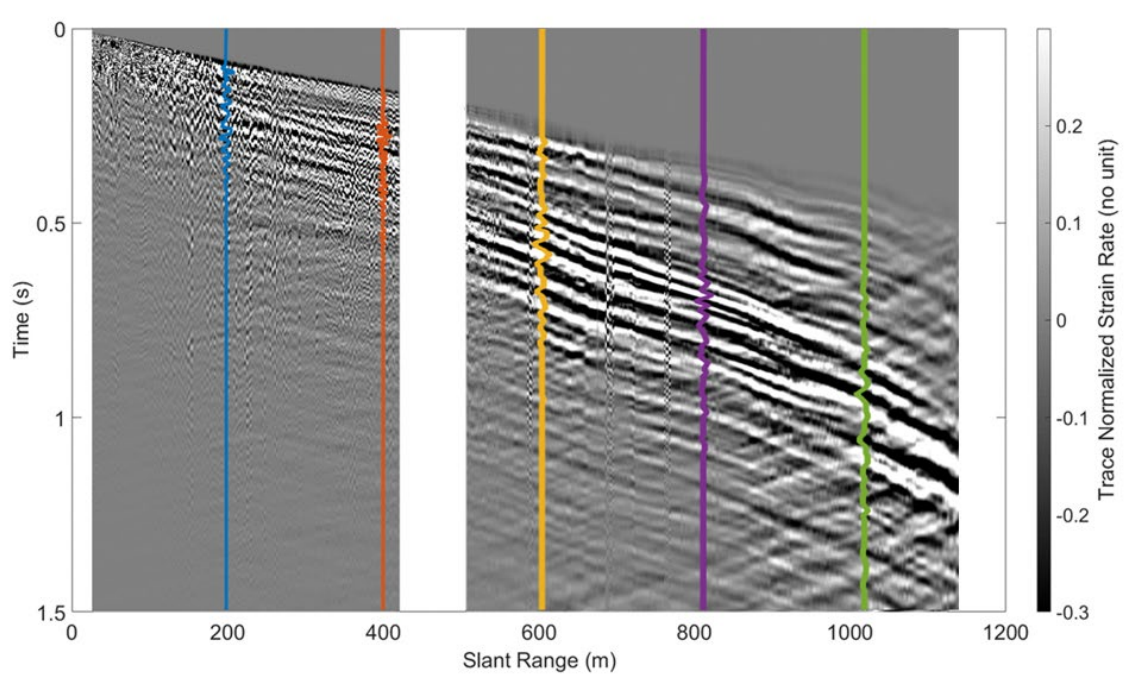


Figure 17. Trace normalized DAS data overlain by the waveforms at multiple ranges in the surface sections of the straight cable. Waveform amplitudes are multiplied by a factor of 10 to make them visible on this figure.

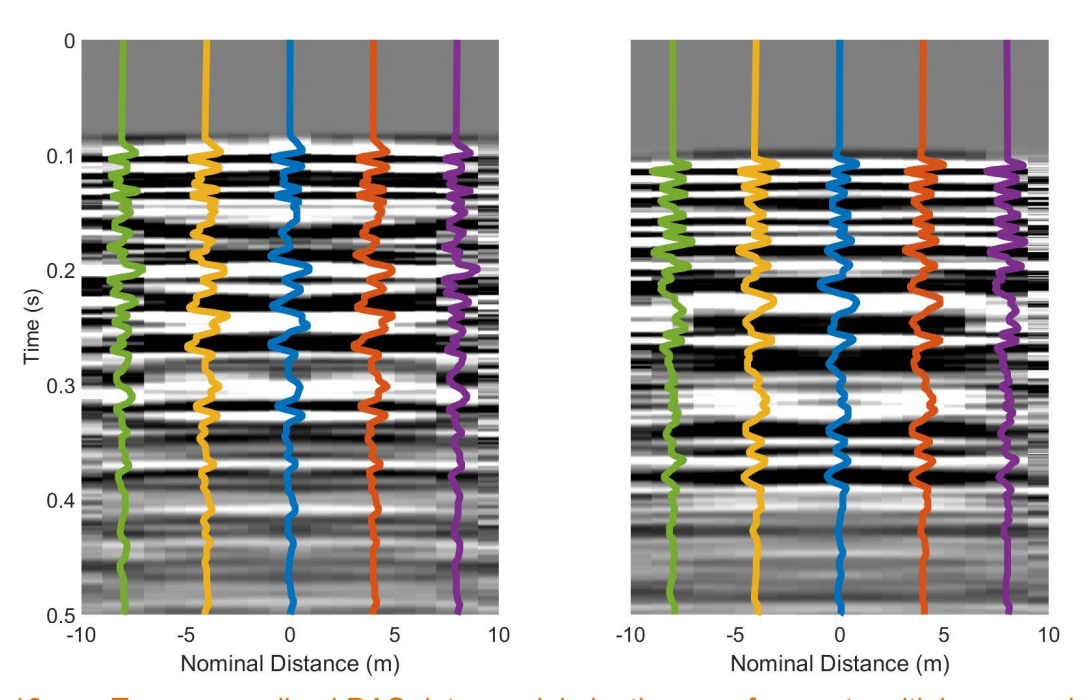


Figure 18. Trace normalized DAS data overlain by the waveforms at multiple ranges in the surface sections of the straight cable in the borehole at 206 m slant range (left column) and 239 m slant range (right column). Waveform amplitudes are multiplied by a factor of 10 to make them visible on this figure. The depth convention for this figure is explained in Figure 14.

6.0 Late Time Observations

Late time observations in this data set include aftershock signals that occurred in both the .06 Bypass and the P-Main drifts. An example of an aftershock in the P-Main drift is shown in Figure 19Figure 19. Of additional note in this portion of the data set, there was a regional earthquake signal at 16:28:48.400Z (not shown in Figure 19).

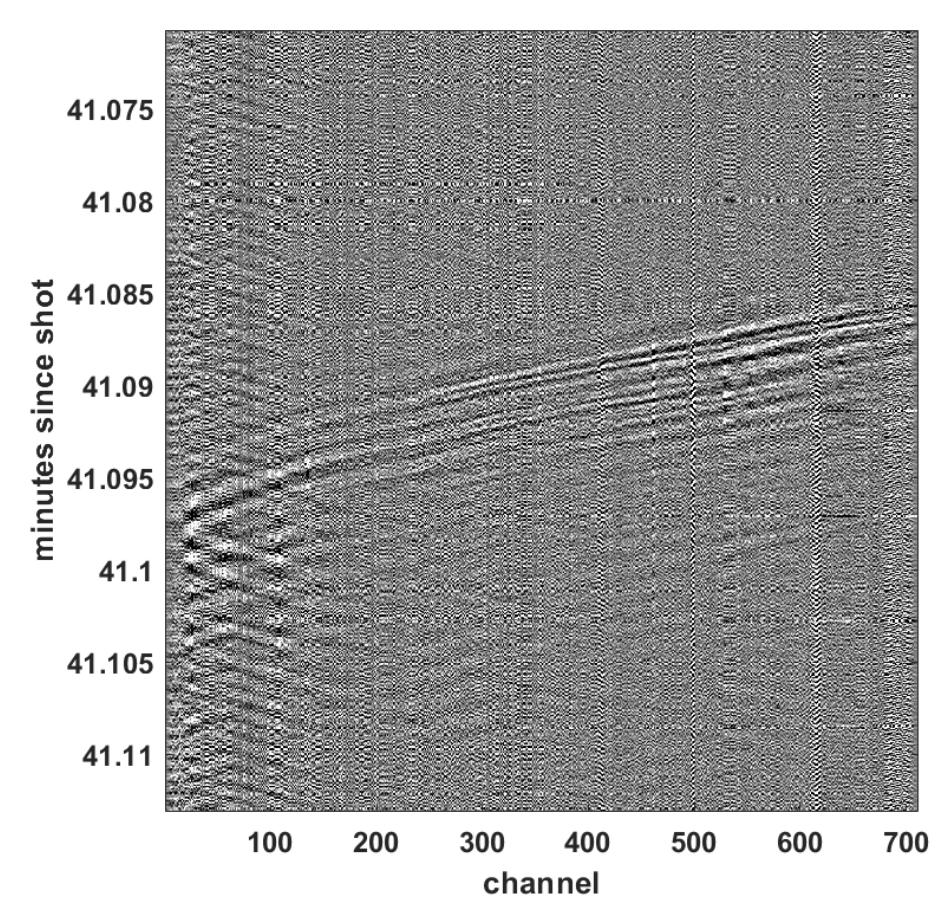


Figure 19. Trace normalized DAS data showing an example of an aftershock in the P-Main drift.

Explosions can trigger sequences of aftershocks that cluster in time and space. Aftershock events following PE1-A were numerous and well recorded along fibers in both the .06 Bypass (Figure 20) and P-Main drifts. Figure 21 shows an aftershock recorded by the helical .06 Bypass fiber approximately 1.5 minutes after PE1-A. Since channel numbers on the right of Figure 21 are closer to the PE1-A explosion (channel 421 is closest to the source) the moveout suggests a southward traveling wave down the .06 Bypass drift to channel 0—the furthest channel from the source. Most of the observed aftershocks had similar moveouts indicating they were originating from a similar location. Clear P-wave arrivals were observed for several hundred meters away from the channel closest to the source. At least two other phases arrived after the P-wave and further down the drift. Given their arrival times, offset, and amplitude relative to the P-wave, these were likely mesa surface reflections and tunnel ground surface waves.

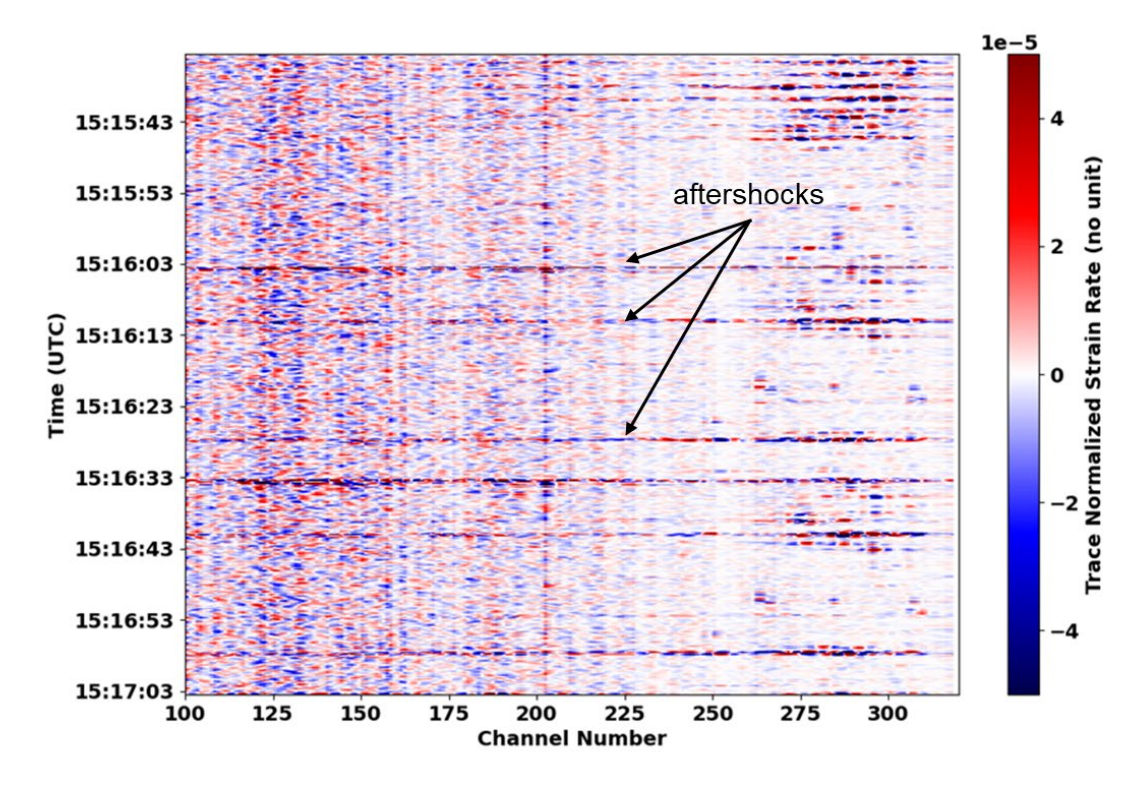


Figure 20 Trace normalized DAS image showing numerous aftershocks in a 45 second window recorded by fiber in the .06 Bypass drift.

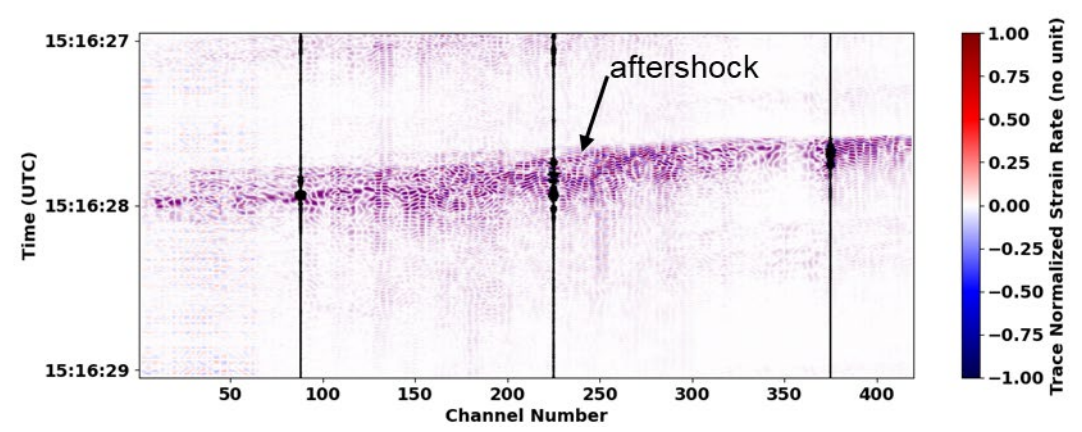


Figure 21 Trace normalized DAS image showing a single aftershock recorded by fiber in the .06 Bypass drift. Data from three separate channels are extracted and overlain as time series on top of the DAS image (black lines).

To determine the number of aftershocks that occurred after the event, a synchrosqueezed continuous wavelet transform (SS-CWT) was used to build a characteristic energy function for both detection and arrival time estimation from a selected channel along the fiber (Daubechies et al., 2011). This analysis detected 305 aftershock events recorded by the .06 Bypass fiber channel closest to the PE1-A source (channel 420) within a 6-hour period following the explosion. However, this is likely an underestimate of the actual number of aftershocks, as a

conservative threshold was chosen to limit the number of spurious events that were chosen. Moreover, a separate template matching analysis on these data resulted in more than double this number of aftershocks during a similar time interval (not shown). Given that variability, the number of aftershocks detected with the SS-CWT method are shown in Figure 22 and binned as the number of minutes after PE1-A for 6-hour and 1-hour time windows respectively.

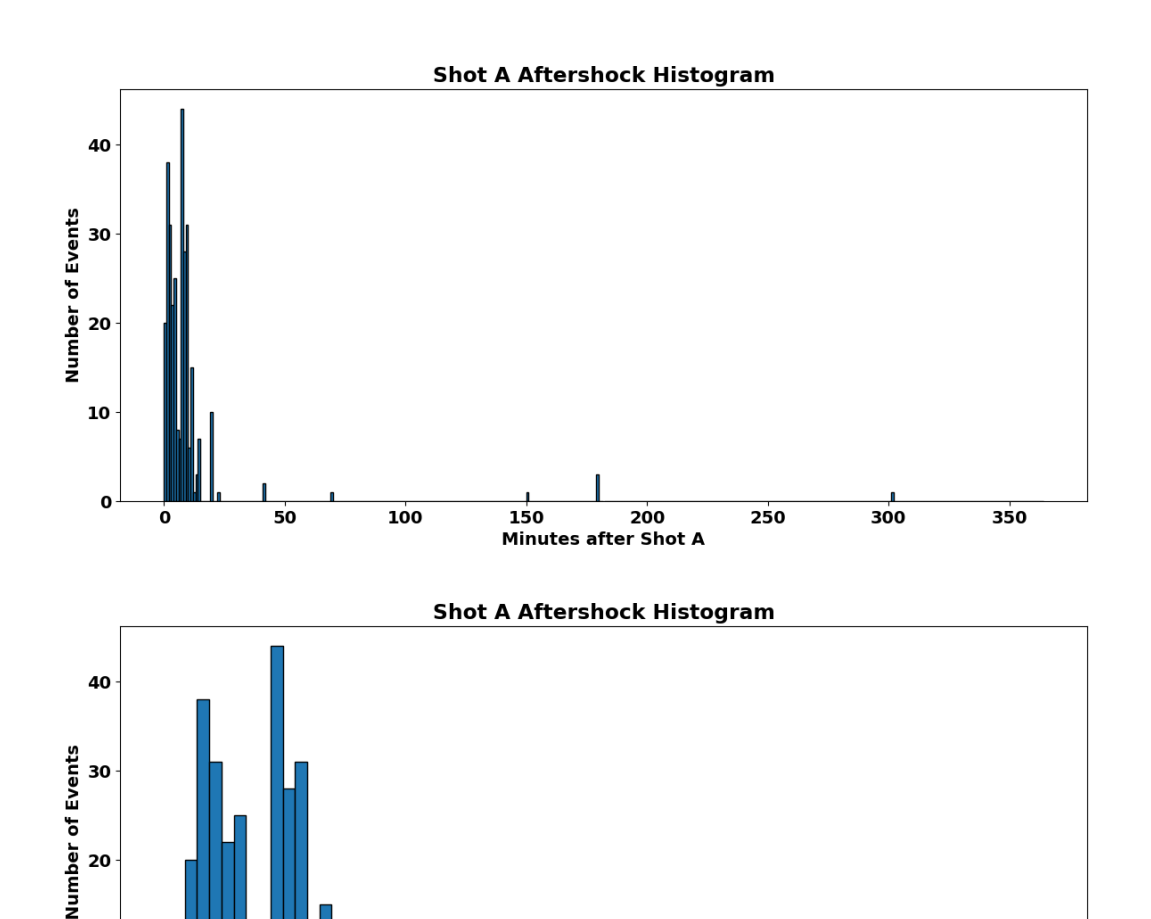


Figure 22 a) Histogram of aftershock activity for the 6-hour period following PE1-A. b) Aftershock histogram for 1-hour period following PE1-A.

30 40 Minutes after Shot A

50

60

70

10

7.0 Summary and Conclusion

DAS successfully recorded ground motion associated with a 16.3 -ton TNT equivalent chemical explosion that occurred on 18 October 2023 in the P-Tunnel complex of the NNSS as the first in a series of explosions for the LYNM PE1 series. The observations were made on a multi-part DAS installation that was designed to explore ground motion from each explosion in the series and compare ground motion across all explosions in the series. Two cables, one with a straight fiber and one with a helically wound fiber, were installed in shallow trenches from 27 m to 1123 m slant range to PE1-A. DAS was recorded at 100 kHz in the section from 27 m to 405 m and 80 kHz in the section from 550 m to 1123 m slant range.

DAS successfully captured three orders of magnitude in strain rate in the first 1.5 seconds after the explosion corresponding with over an order of magnitude in frequency content. The fiber saturated in the first 27 m to 186 m slant range, but the primary as well as later phases of the wavefield were recorded coherently across the rest of the fiber installation. The peak values of measured strain rates thereafter varied three orders of magnitude from 2.0 x 10⁶ nm m⁻¹ s⁻¹ to 7.9 x 10³ nm m⁻¹ s⁻¹ over a range of 187 m to 1123 m in the first 1.5 seconds after the explosion. Peak frequency contents appeared broad band for the saturated region, then reduced from 120 Hz at a range of 187 m to 50 Hz at a range of 1123 m in the first 1.5 seconds after the explosion. Measured strain rate amplitudes compared favorably with strain rates calculated from two of the three geophone and accelerometer pairs that were each recorded at 1 kHz and colocated with the fiber. DAS performed with comparable sensitivity to the geophones and accelerometers in this experiment. The variation with the third pair is under investigation.

These results indicate that near-source DAS observations can refine interpretations of phase identification from single-point sensor observations of explosion-generated seismic wavefields. Traditionally, first arrivals may be attributed to the same P-phase of the wavefield observed by single point sensors very close to the source; however, at larger distances that arrival may represent a variety of different phases dependent on the structure in the travel path. Phase misidentification may be a mechanism responsible for apparent interstation variability near the source and possibly at larger distances as propagation effects may differentially operate on aspects of the group of first arriving phases. This could be one mechanism that contributes scatter to single point seismic measurements which would confound the performance of empirical relationships for small explosions. Removing that mechanism may therefore reduce interstation variability and increase empirical relationship performance for small explosions.

This study adds to that body of work reporting near-source DAS observations of the seismic wavefields generated by underground chemical explosions. These results for downhole DAS sections are consistent with previous work which noted that downhole DAS data can provide improved characterization of underground explosion-derived seismic wavefields (Porritt et al, 2023). This study extends that finding to surface DAS installations that are horizontal in tunnels at much closer scaled ranges. The scaled range for this installation was 354 – 14,533 m kT^{-1/3}, without using a pre-multiplying constant of two. Future work will explore the late-time observations and analyze the observations at early and late times to better understand PE1-A explosion phenomenology and compare the results of this event with other explosive events recorded with DAS as well as results from empirical theoretical models.

8.0 References

Abbott, R., R. Mellors, and A. Pitarka. 2019. Distributed Acoustic Sensing Observations and Modeling of the DAG series of chemical explosions. Conference Presentation. SAND2019-5816C https://www.osti.gov/biblio/1640162.

Bodmer, M. et al., 2024. LYNM PE1 Pre-Experiment A Site Characterization Report, Technical Report, SAND2024-07522/PNNL-36326.

Lindsey, N. J., H. Rademacher, and J. B. Ajo-Franklin. 2020. On the Broadband Instrument Response of Fiber-Optic DAS Arrays, Journal of Geophysical Research: Solid Earth, Vol. 125, Issue 2 https://doi.org/10.1029/2019JB018145

Kuvshinov, B. N. 2016. Interaction of helically wound fibre-optic cables with plane seismic waves. Geophysical Prospecting, 64(3), 671–688. https://doi.org/10.1111/1365-2478.12303

Mellors, R. J., R. Abbott, D. Steedman, D. Podrasky, and A. Pitarka. 2021. Modeling Subsurface Explosions Recorded on a Distributed Fiber Optic Sensor, Journal of Geophysical Research: Solid Earth, Vol. 126. Issue 12, https://doi.org/10.1029/2021JB022690

Myers, S. C. et al. A multi-Physics Experiment for Low-Yield Nuclear Explosion Monitoring. United States: N. p., 2024. Web. doi:10.2172/2345984.

Porritt, R. W.; R. E. Abbott, C. Poppeliers. 2022. Quantitative assessment of Distributed Acoustic Sensing at the Source Physics Experiment (Phase II), Technical Report, https://doi.org/10.2172/1855336

Veins, L., and B. G. Delbridge. 2024. Shallow Soil Response to a Buried Chemical Explosion With Geophones and Distributed Acoustic Sensing, Journal of Geophysical Research: Solid Earth, Vol. 129, Issue 7, https://doi.org/10.1029/2023JB028416

Walter, W. R., M. Begnaud, C. E. Seifert, and S. Teich-McGoldrick. 2023. The Low-Yield Nuclear Monitoring (LYNM) Experimental Science Plan. Web. doi:10.2172/1983733.

Daubechies, I., J. Lu, and H. T. Wu. 2011. "Synchrosqueezed wavelet transforms: an empirical mode decomposition-like tool." *Applied and Computational Harmonic Analysis*. Vol. 30(2), pp. 243–261. https://doi.org/10.1016/j.acha.2010.08.002.

Pacific Northwest National Laboratory

902 Battelle Boulevard P.O. Box 999 Richland, WA 99354

1-888-375-PNNL (7665)

www.pnnl.gov